ResearchGate

See discussions, stats, and author profiles for this publication at: https://www.researchgate.net/publication/286403705

Climate mechanism for stronger typhoons in a warmer world

Article *in* Journal of Climate · December 2015

DOI: 10.1175/JCLI-D-15-0585.1

CITATIONS
2

READS
59

2 authors:

Nam-Young Kang
Korea Meteorological Administration
10 PUBLICATIONS 34 CITATIONS

SEE PROFILE

James B. Elsner
Florida State University
216 PUBLICATIONS 6,020 CITATIONS

SEE PROFILE

Some of the authors of this publication are also working on these related projects:

Project Statistical models for tornado climatology View project

All content following this page was uploaded by James B. Elsner on 15 December 2015.

The user has requested enhancement of the downloaded file.

Climate mechanism for stronger typhoons in a warmer world

Nam-Young Kang,[1,*] and James B. Elsner[2,3]

[1]*National Typhoon Center / Korea Meteorological Administration, Jeju, S. Korea*

[2]*Department of Geography, Florida State University, Tallahassee, Florida, USA*

[3]*Geophysical Fluid Dynamics Institute, Florida State University, Tallahassee, Florida, USA*

[*]*Corresponding author address:* 2 Seosung 810-gil, Namwon , Seogwipo, Jeju, 699-942, S. Korea

E-mail: nkang.fsu@gmail.com

ABSTRACT

Violent typhoons continue to have catastrophic impacts on economies and welfare but how they are responding to global warming has yet to be fully understood. Here we use an empirical framework to explain physically why observations support a tight connection between increasing ocean warmth and the increasing intensity of super typhoons in the western North Pacific. We show that the energy needed for deep convection is on the rise with greater heat and moisture in the lower tropical troposphere but that this energy remains untapped when air pressure is high. Accordingly, tropical cyclone formation is becoming less common but those that do form are likely to reach extreme intensities from the discharge of stored energy. These thermodynamic changes to the environment most significantly influence the upper portion of extreme typhoon intensities indicating that super typhoons are likely to be stronger at the expense of overall tropical cyclone occurrences in the western North Pacific.

1. Introduction

The changing nature of tropical cyclone (TC) climate is an important concern in relation to anthropogenic global warming. In particular, the western North Pacific accounts for about one third of all TCs worldwide (Chan 2005). The recent onslaught of super typhoons makes countries tense from anticipation about future TC activity. Super typhoon Haiyan in 2013 struck the Philippines and destroyed more than a million houses killing 6,300 people (NDRRMC 2014). Even super typhoon Vongfong and Hagupit in 2014 rapidly developed into typhoons with intensities comparable to Haiyan. Over a million people were evacuated in the Philippines by the threat of Hagupit. People may suspect that global warming has a connection with TCs becoming violent in this ocean basin. Trends in annual TC occurrence rates have been investigated (Webster et al. 2005), but the influence of global warming is difficult to detect against the background of natural variation (Chan 2006, 2008). Additionally observed trends can result simply from improvements in the quality of observations (Kossin et al. 2013) and estimated trends depend on the range of years considered (Klotzbach 2006). A long period of record is preferable but there is no guarantee of reduced uncertainty. For these reasons TC climate studies have tended toward a reliance on numerical model simulations (Knutson et al. 2010). Yet results from these studies remain inconclusive (IPCC 2012).

Here we provide a physical explanation for how extreme TCs in the western North Pacific respond to global warming and to their large scale environments. New understanding is made possible by using an empirical framework with a consistent set of reliable observations (Kang and Elsner 2012a,b). The framework is motivated by the link between TC frequency and intensity (Emanuel 2008; Elsner et al. 2008). By projecting global ocean temperature variation onto a two-dimensional continuous frequency-intensity space (Kang and Elsner 2015), we are able to give an integrated assessment of typhoon climate. Section 2 describes the data and framework. Section 3 shows the statistical results and section 4 explains them physically. Section 5 describes the connection between super typhoons and global ocean warmth. Section 6 provides summary of the results and a discussion. All the statistics and figures are created using the software R (`www.r-project.org`) and are available from `rpubs.com/Namyoung/P2015a`.

2. Methodology

a. Data

We first organize a set of TC best-tracks from the U.S. Joint Typhoon Warning Center (JTWC, `www.usno.navy.mil/NOOC/nmfc-ph/RSS/jtwc/best_tracks`) and the Japan Meteorological Agency (JMA, `www.jma.go.jp/jma/jma-eng/jma-center/rsmc-hp-pub-eg/trackarchives.html`). More than one TC dataset is available in the western North Pacific. Different observation procedures by different operational agencies create inconsistencies in the values within the dataset over time. For example, prior studies have tried to find a consensus among the estimated TC intensities from the various agencies (Song et al. 2010; Knapp and Kruk 2010) by matching individual TC events. But this turns out to be a difficult task.

Another problem is that analysis results using a particular dataset tend to vary according to the period of data used. A long period is preferred to minimize statistical uncertainty but this comes at the expense of uneven data quality. A compromise is a selection of a useful period that contains as many reliable observations as possible. The longest period of reliable western North Pacific TC data is one that extends back to 1984 (Kang and Elsner 2012b). The data consist of lifetime-maximum winds (LMWs) from TCs during June through November (JJASON) over the 30-year period 1984–2013. Other environmental variables such as sea surface temperature (SST), Southern Oscillation Index (SOI), air temperature, specific humidity, and geopotential height come from the

National Oceanic and Atmospheric Administration (NOAA) National Centers for Environmental Prediction (NCEP) reanalysis (`www.esrl.noaa.gov/psd/data/gridded`). Specifically, we utilize monthly SSTs from Extended Reconstructed Sea Surface Temperature (ERSST) V3b. SOI comes from the the NOAA Climate Prediction Center (CPC, `www.cpc.ncep.noaa.gov/data/indices/soi`).

b. Framework

To investigate TC climate variability we first define equally contributing indicators. A schematic diagram for our framework Kang and Elsner (2012a,b) is shown in Figure 1. INT is the annual mean intensity of TCs having lifetime-maximum winds (LMWs) exceeding a threshold quantile. The lowest threshold quantile (zero empirical probability level—probability of a TC having weaker winds) is set as 17 m s^{-1}. INT can be computed at successively higher thresholds. FRQ is the annual number of TCs above each successive threshold. By definition the variation of FRQ is not affected by the probability level. For example, the FRQ variation of the 50 % strongest portion of TCs is the same as that of the total TCs. INT is on the horizontal axis and FRQ is on the vertical axis.

An annual value in the upper-right quadrant represents high values of INT and FRQ, while an annual value in the lower-left quadrant represents low values of INT and FRQ. Thus a positive diagonal line provides an axis that captures the in-phase relationship between INT and FRQ that we denote ACT. ACT can be obtained by principal component analysis and is computed as

$$\mathrm{ACT} = \left(\frac{\mathrm{INT} - \mu_{\mathrm{INT}}}{\sigma_{\mathrm{INT}}} + \frac{\mathrm{FRQ} - \mu_{\mathrm{FRQ}}}{\sigma_{\mathrm{FRQ}}} \right) / \sqrt{2}, \tag{1}$$

where INT and FRQ are vectors of annual values. μ and σ denote their respective mean and standard deviations. ACT indicates the in-phase relationship between INT and FRQ, which is comparable to TC energy as indicated by its high correlation (Kang and Elsner 2012a) with Accumulated Cyclone Energy (ACE) (Bell et al. 2000) and Power Dissipation Index (PDI) (Emanuel 2005). On the other hand, a value in the upper-left quadrant is characterized by low INT and high FRQ, and a value in the lower-right quadrant shows high INT and low FRQ. Thus a negative diagonal line provides an axis that captures the out-of phase relationship between INT and FRQ. This variability is denoted as EINT, which expresses the efficiency of intensity. Alternatively the negative EINT can be understood as the efficiency of frequency. EINT is the other principal component and is computed as

$$\mathrm{EINT} = \left(\frac{\mathrm{INT} - \mu_{\mathrm{INT}}}{\sigma_{\mathrm{INT}}} - \frac{\mathrm{FRQ} - \mu_{\mathrm{FRQ}}}{\sigma_{\mathrm{FRQ}}} \right) / \sqrt{2}. \tag{2}$$

Owing to the presence of EINT, a continuous two-dimensional variability space is formed, where the center is the mean of each standardized set of FRQ and INT values. Now, an annual TC climate can be indicated by a single point in the continuous variability space. In this framework, variability in any direction can be defined as

$$\mathrm{TCI}_{\theta} = \mathrm{INT} \cdot \cos\theta + \mathrm{FRQ} \cdot \sin\theta, \tag{3}$$

where TCI denotes a directional variability (θ) away from INT (positive is counterclockwise), which represents the weighted linear combination of FRQ and INT. ACT and EINT are the special cases when θ is $+45$ and -45, respectively.

3. Correlation Screen

Figure 2 illustrates the empirical framework and the correlation circle for the strongest 10 % (.9 probability level—90% of the TCs have winds weaker than this) of western North Pacific TCs based on 30 years of JJASON observations. The average wind speed for this subset is 67 m s^{-1} using the JTWC dataset, which nearly matches the super typhoons of category 5 on the Saffir-

Simpson scale (Simpson 1974). The quantile method is useful for dealing with intensity variation of fewer events (Elsner et al. 2008). With an increase in super typhoon intensities, the threshold LMW of the strongest 10 % of TCs increases above 67 m s^{-1} and INT over the threshold increases. The average wind speed of the strongest 10 % of TCs using the JMA dataset is 49 m s^{-1}. On the other hand, the variation in FRQ is not affected by the probability level by definition. The annual variation in the number of all TCs should match the annual variation in the number of just the top 10 % of them. Since this quantile approach controls INT only, the interpretation of the empirical framework centers on the relationship between overall TC occurrences and the intensity of the upper 10 % subset.

Circular direction in Fig. 2 represents each TC climate variability, where INT and FRQ have different weights by an angle (see Eq. 3). Correlations are calculated for each directional variability of TC climate with global ocean warmth (indicated by global mean SST). Each 30-year (1984–2014) annual value for JJASON is used. The vector of global mean SST is fixed, but a vector of TC climate varies by each angle. Finally, the correlation between TC climate and global ocean warmth is mapped with a loop on the correlation screen. Correlation shows the similarity of this environment to another synthetic environment that global ocean warmth brings about. The purple loop is the correlation using data from JTWC and the green loop is the correlation using data from JMA. The thick orange/red loop is the correlation using composite data from the JTWC and JMA. Center, inner circle and outer circle in gray color indicate the correlation levels of 0, 0.5 and 1, respectively.

Principal component analysis is used to composite JTWC and JMA observations. FRQ and INT are the principal components which indicates the in-phase relationship between the two observations. FRQ is represented as

$$\mathrm{FRQ} = \left[\mathrm{s}\left(\mathrm{FRQ}_{\mathrm{JTWC}}\right) + \mathrm{s}\left(\mathrm{FRQ}_{\mathrm{JMA}}\right)\right] / \sqrt{2}, \tag{4}$$

where the operator 's( )' returns standardized values of an input vector as expressed in Eqs. 1 and 2. Likewise, INT is represented as

$$\mathrm{INT} = \left[\mathrm{s}\left(\mathrm{INT}_{\mathrm{JTWC}}\right) + \mathrm{s}\left(\mathrm{INT}_{\mathrm{JMA}}\right)\right] / \sqrt{2}. \tag{5}$$

The highest correlation (r = +0.75 [0.53, 0.87] 95 % CI) occurs in the EINT direction (red dot). The statistically significant correlation range is indicated in red. As defined, higher INT can occur in years with higher EINT and higher ACT, and lower FRQ in years with higher EINT and lower ACT. However, since EINT is orthogonal to ACT it represents the out-of-phase relationship between INT and FRQ. Thus, the strong correlation along the EINT direction makes it clear that global ocean warmth influences the *collinearity* between INT and FRQ rather than influencing ACT alone or either INT or FRQ individually.

4. TC Environment

Increasing EINT (fewer TCs, but stronger super typhoons) is an empirical result that arises from synchronous changes to physical factors under the influence of global warming (see Fig. 2). A decrease in FRQ together with an increase in INT results from an increase in saturation deficit occurring in the tropical free atmosphere in concert with a decrease in upward mass flux. Figure 3 shows that the climate dynamics for the global tropics explained by Kang and Elsner (2015) is also valid and even more apparent in the tropical region of the western North Pacific. Here, specific humidity and geopotential height as well as air temperature are used for the plot with data coming from the NCEP reanalysis. To find a clear response of the regional environment to global ocean warmth, ENSO influence (indicated by a negative SOI value) is statistically removed from variables and the partial correlation is calculated. Then we determine western North Pacific TC environment at the same ENSO conditions (statistically) when global ocean warmth is increasing. In globally warm years regional SSTs across the tropical western North Pacific are also above normal. The increase in regional SST itself is a positive environmental factor for ACT. As warmth increases, the lower troposphere in this region gains additional moisture following the Clausius-Clapeyron relationship. However, aloft in the free atmosphere the moisture gain is less (Held and Soden 2006). This is different from temperature changes in the middle and upper troposphere, which increase significantly by convection following a moist adiabat (Chou et al. 2013). Though the temperature is also influenced by dynamic and radiative processes, the major change is driven by the moist convection. The vertical profile of correlation confirms that moist static energy increases in the western North Pacific tropics (100°E–180°, 0°–30°N) are more pronounced in the lower troposphere under increasing global temperature. This environmental change implies a convectively more unstable troposphere which leads to more ACT (greater FRQ and INT).

In contrast, regionally increasing air pressure aloft (at a constant geopotential height) inhibits ACT. Unlike in the lower troposphere where pressure is influenced by the air mass above, in the middle and upper troposphere pressure is directly influenced by air temperature. The vertical profiles of correlation show that geopotential height is strongly co-linear with higher SST implying a cap on the destabilized troposphere. Since temperature is well stratified the air-pressure anomaly over the middle and upper troposphere is also stratified leading to a decrease in the upward mass flux (Sugi and Yoshimura 2012). If high pressure aloft is dominant then convection has limited opportunity to transport energy from the lower troposphere leading to fewer TCs. Yet considering the large moist static energy the limited opportunity implies stronger TCs for those that do form (Kang and Elsner 2015). Therefore, as demonstrated by the large and significant correlation between western North Pacific EINT and global temperature, we can conclude that the convectively destabilized troposphere with large moist static energy in this region accompanied by a strong pressure anomaly aloft inhibits overall TC occurrences but TCs that do form are likely to obtain greater intensity (on average) resulting from the discharge of additional energy.

Figure 4 shows correlation maps of global ocean warmth with regional SST and regional geopotential height at 500 hPa, where partial correlation is computed at each grid point. Compared with Fig. 5 where ENSO variation is not removed, the regional SST is seen to be even more pronounced. Enhanced regional SST anomalies accompanying the global ocean warmth variation provides a better understanding of the anomalous high.

5. Time Series of Global Ocean Warmth and the 10 % Strongest Typhoons

As INT is the combination of ACT and EINT, EINT implies the portion of INT which is not influenced by ACT. In other words, EINT represents the INT variation (the negative FRQ variation at the same time) where an internal variation, ACT, is removed. Trends and annual fluctuations over the 30-year period (1984–2013) confirm a tight connection between global ocean warmth and EINT at this extreme portion (Fig. 6). The trend of standardized SST over the period is $+2.8 \pm 0.37$ (s.e.) s.d./30 yr which compares with the trend in EINT of $+2.0 \pm 0.52$ (s.e.) s.d./30 yr. The correlation between the two series is $+0.75$ [0.53, 0.87] 95 % CI that reduces to $+0.57$ [0.25, 0.77] 95 % CI after removing the linear trends. The results clarify that super typhoons are likely to become stronger at the expense of overall TC frequencies in a warmer world regardless of variations to ACT. The time series of global ocean warmth (red line) indicates how the TC environments have evolved to enhance the intensity of super typhoons in the western North Pacific. Standardized EINT values are averaged to be -0.12 and 0.75 (s.d.) for each of the last two decades, confirming the recent TC climate feature of lowering frequency but stronger intensity.

6. Summary and Discussion

Among the TC climate variability directions, we find that EINT for the 10 % of the most intense TCs is strongly influenced by global ocean warmth. The thermodynamic structure of the tropical western North Pacific with high global ocean warmth is characterized by convectively more unstable lower troposphere, but simultaneously prevailing high pressure anomaly in the middle and upper troposphere. Increasing EINT in a warmer year shows that this environment further inhibits the TC occurrences over the region, but TCs that form tend to discharge stored energy to the upper troposphere with stronger intensities. As the increasing intensities compensate for the loss of ACT by decreasing number of TCs, the ACT remains largely unchanged. As the strongest 10 % of the TCs are on average comparable to super typhoons, the increasing EINT suggests clearly that super typhoons in warmer years get stronger. The study is unique in that it does not use smoothing or wavelet transforms. It explores directly the annual variation of TC climate with global SST, which is a useful indicator of global ocean warmth. Thus, it is not necessary to assume an increasing trend as the influence of global warming. In contrast to the classical way of trend analysis, here global warming influences on the two best-tracks in JJASON are compared to find a reliable TC climatology. In addition, this study clarifies the background thermodynamics by computing partial correlations on the environmental variables.

Assuming the warming trend in the oceans continue, this study implies we will likely experience a year warmer than ever and thus a larger EINT. By definition a larger EINT means a larger gap between intensity and frequency with the consequence of record strong super typhoons at the expense of fewer overall TCs. Figure 7 summarizes the findings from a linear perspective. TC activity is demonstrated as a variation that is independent of global warming, and can be assumed to be internal variability having no trend. Frequency variation and super typhoon intensity variation are regarded as the addition of global warming influence on TC activity variation. The structure depicts how a previous intensity record is overtaken while frequency falls in our global warming environment. A year with record global ocean warmth is likely to experience a record-breaking intensity even during a lull in TC activity.

Acknowledgments. This work was supported by the National Typhoon Center at the Korea Meteorological Administration and Geophysical Fluid Dynamics Institute at the Florida State University.

References

Bell, G. D., and Coauthors, 2000: Climate Assessment for 1999. *Bull. Am. Meteorol. Society.*, **81 (6)**, s1–s50.

Chan, J. C. L., 2005: Interannual and interdecadal variations of tropical cyclone activity over the western North Pacific. *Meteorol. Atmos. Phys.*, **89**, 143–152.

Chan, J. C. L., 2006: Comment on "Changes in Tropical Cyclone Number, Duration, and Intensity in a Warming Environment". *science*, **311**, 1713.

Chan, J. C. L., 2008: Decadal variations of intense typhoon occurrence in the western North Pacific. *Proc. R. Soc.*, **464**, 249–272.

Chou, C., T. C. Wu, and P. H. Tan, 2013: Changes in gross moist stability in the tropics under global warming. *Clim. Dyn.*, **41**, 2481–2496.

Elsner, J. B., J. P. Kossin, and T. H. Jagger, 2008: The increasing intensity of the strongest tropical cyclones. *Nature*, **455**, 92–95, doi:10.1038/nature07234.

Emanuel, K. A., 2005: Increasing destructiveness of tropical cyclones over the past 30 years. *Nature*, **436**, 686–688.

Emanuel, K. A., 2008: The hurricane-climate connection. *Bull. Am. Meteorol. Soc.*, **89**, ES10–ES20.

Held, I. M., and B. J. Soden, 2006: Robust Responses of the Hydrological Cycle to Global Warming. *J. Clim.*, **19**, 5686–5699.

IPCC, 2012: Fifth assessment report. www.ipcc.ch/report/ar5/wg1, 1252 pp.

Kang, N.-Y., and J. B. Elsner, 2012a: An empirical framework for tropical cyclone climatology. *Clim. Dyn.*, **39**, 669–680, doi:10.1007/s00382-011-1231-x.

Kang, N.-Y., and J. B. Elsner, 2012b: Consensus on Climate Trends in Western North Pacific Tropical Cyclones. *J. Clim.*, **25**, 7564–7573.

Kang, N.-Y., and J. B. Elsner, 2015: Trade-off between intensity and frequency of global tropical cyclones. *Nature Clim. Change*, **5**, 661–664.

Klotzbach, P. J., 2006: Trends in global tropical cyclone activity over the past twenty years (19862005). *Geophys. Res. Lett.*, **33**, L10 805.

Knapp, K. R., and M. C. Kruk, 2010: Quantifying interagency differences in tropical cyclone best-track wind speed estimates. *Mon. Wea. Rev.*, **38**, 1459–1473.

Knutson, T. R., and Coauthors, 2010: Tropical cyclones and climate change. *Nature Geosci.*, **3**, 157–163.

Kossin, J. P., T. L. Olander, and K. R. Knapp, 2013: Trend Analysis with a New Global Record of Tropical Cyclone Intensity. *J. Clim.*, **26**, 9960–9976.

NDRRMC, 2014: Updates re the effects of typhoon "yolanda"(haiyan). www.ndrrmc.gow.ph, 2 pp.

Simpson, R. H., 1974: The hurricane disaster potential scale. *Weatherwise*, **27**, 169–186.

Song, J. J., J. Wang, and L. Wu, 2010: Trend discrepancies among three best track data sets of western North Pacific tropical cyclones. *J. Geophys. Res.*, **115**, D12 128, doi:10.1029/2009JD013058.

Sugi, M., and J. Yoshimura, 2012: Decreasing trend of tropical cyclone frequency in 228-year high-resolution AGCM simulations. *Geophys. Res. Lett.*, **39**, L19 805.

Webster, P. J., G. J. Holland, J. A. Curry, and H.-R. Chang, 2005: Changes in tropical cyclone number, duration, and intensity in a warming environment. *Science*, **309 (5742)**, 1844–1846, doi:10.1126/science.1116448.

LIST OF FIGURES

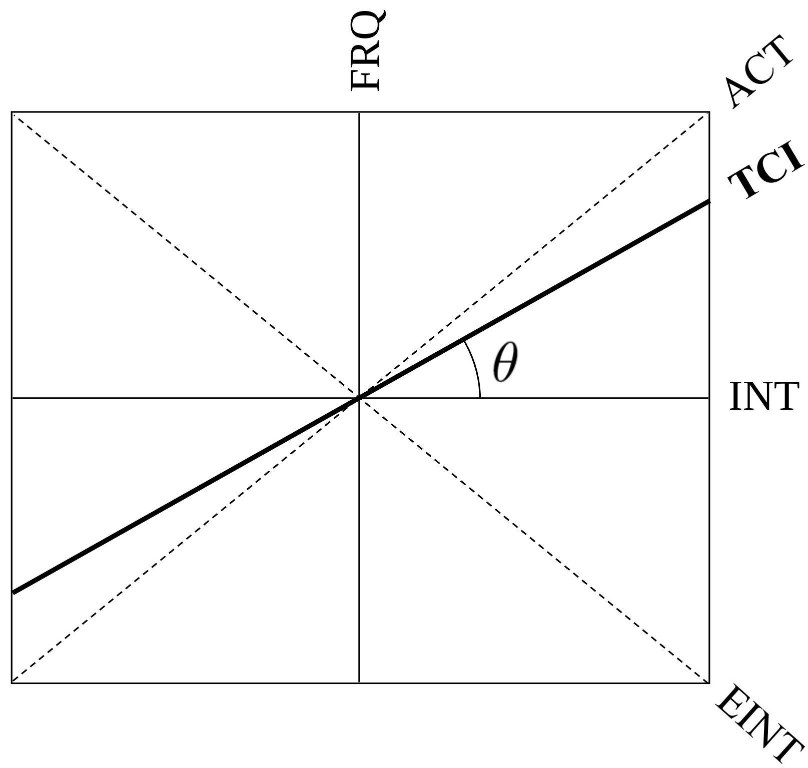

312 Fig. 1. Schematic of our TC climate framework. The positive diagonal (positive slope) captures the level of coherence between FRQ and INT. The negative diagonal (negative slope) captures the level of discordance. The state of the TC climate can be represented as a single point in the two-dimensional variability space. A variability direction of TC climate is shown as a thick black line. θ is the angle starting from INT. ACT and EINT are the special cases when θ is $+45°$ and $-45°$, respectively. ACT and EINT are formed by equal weighting of INT and FRQ.

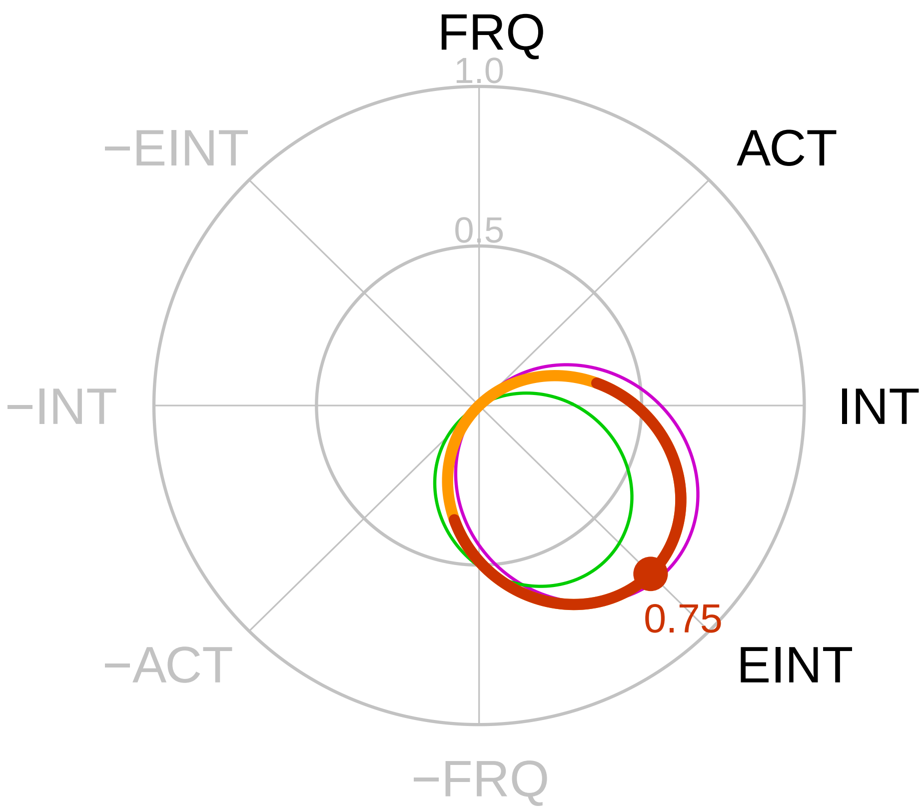

FIG. 2. Correlation screen of global ocean warmth and climate variability using the strongest 10 % of all TCs in the western North Pacific. Global mean SST is used as global ocean warmth indicator. All indicators used for correlations are annual values averaged for JJASON over 30 years (1984–2013). Center, inner circle and outer circle indicate the correlation levels of 0, 0.5 and 1, respectively. Correlations for JTWC and JMA are shown in purple and green loops, respectively. Each loop is a polygon linking 360 correlation values at 1° intervals. The orange line shows the correlation of global ocean warmth with composite TC climate from JTWC and JMA. The red portion of the line represents the significant ($\alpha \leq 0.05$) range of correlations. The dot indicates the direction of the largest correlation.

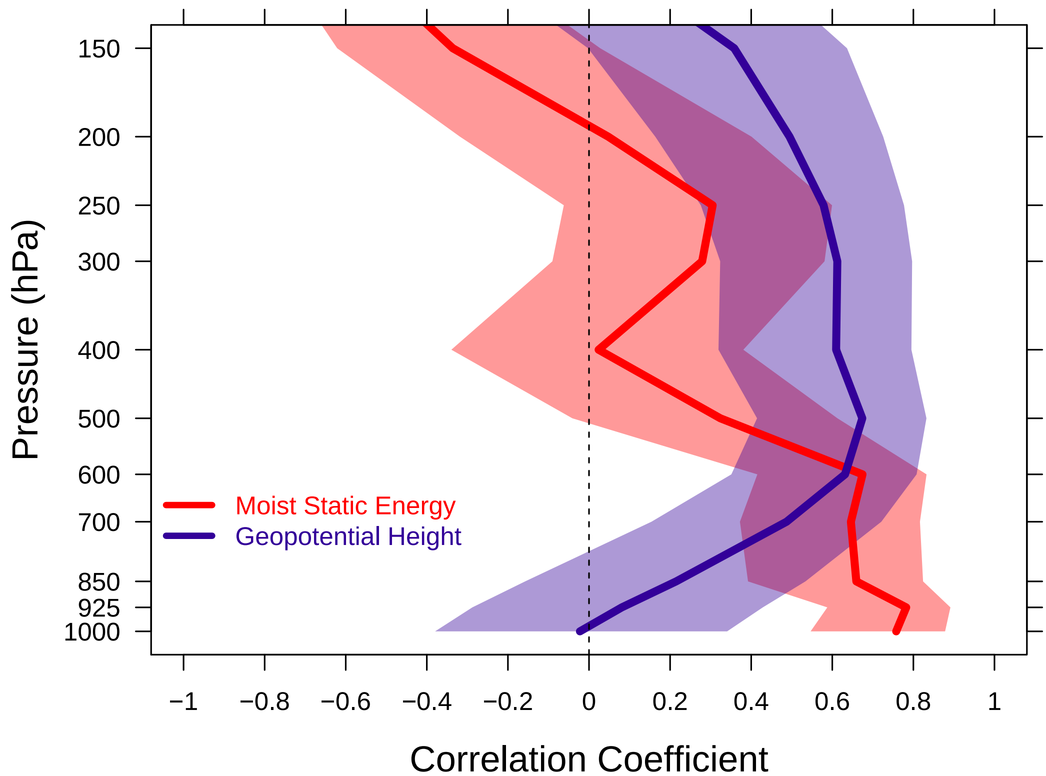

FIG. 3. Correlation profile of global ocean warmth with moist static energy and geopotential height in the tropical region (0°–30°N) of the western North Pacific (100°E–180°). The significant correlation range ($\alpha \leq 0.05$) at each pressure level is shaded. All values are averaged for JJASON over 30 years (1984–2013) to calculate correlations. The ENSO influence is removed separately from each variable so the values represent the partial correlation. The graph shows the thermodynamics of a globally warm environment at the same ENSO condition.

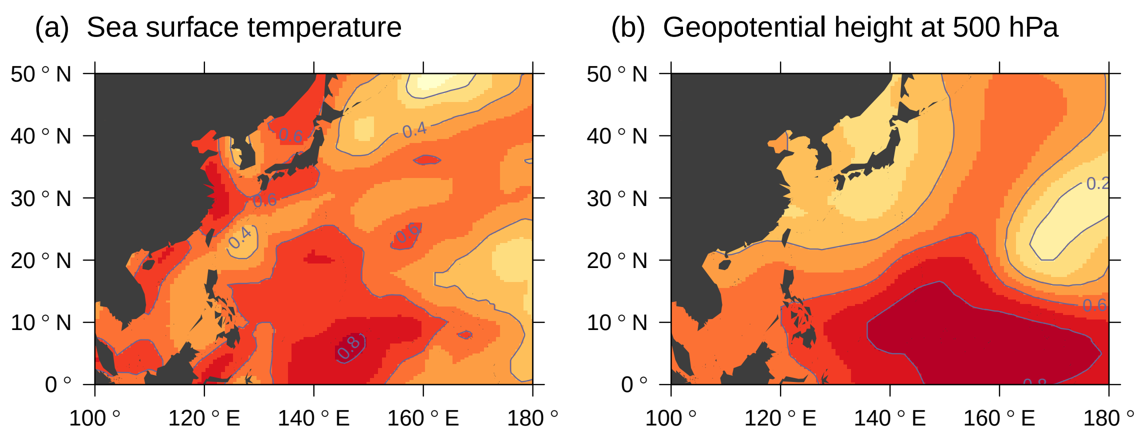

FIG. 4. Correlation maps of global ocean warmth with (a) regional SST and (b) regional geopotential height at 500 hPa. At each grid point, ENSO influence is removed from the variables and partial correlation is calculated. Thus, the result shows the regional pattern of a globally warm environment at the same ENSO condition. Global mean SST is used as an indicator of global ocean warmth. All values are averaged for JJASON over 30 years (1984–2013) to calculate correlations.

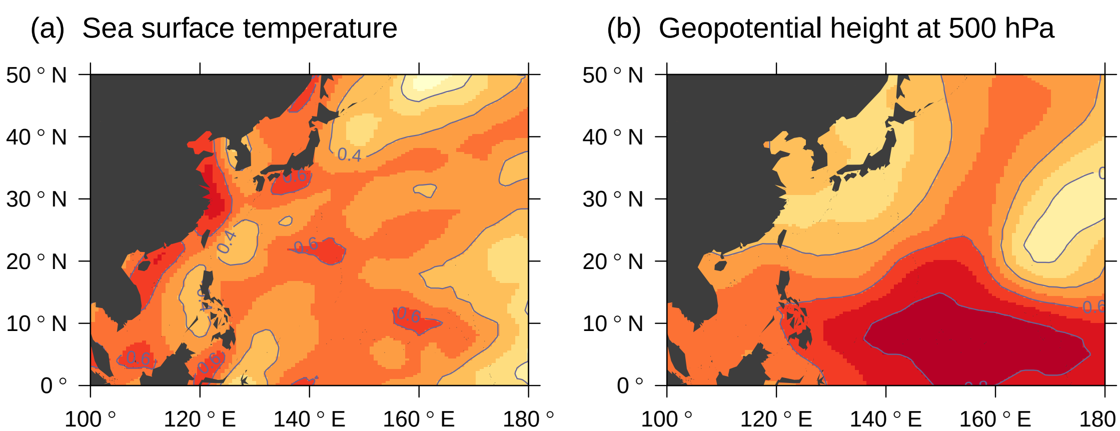

FIG. 5. Same as Fig. 4 but using correlation rather than partial correlation. This is to see the influence of ENSO variation.

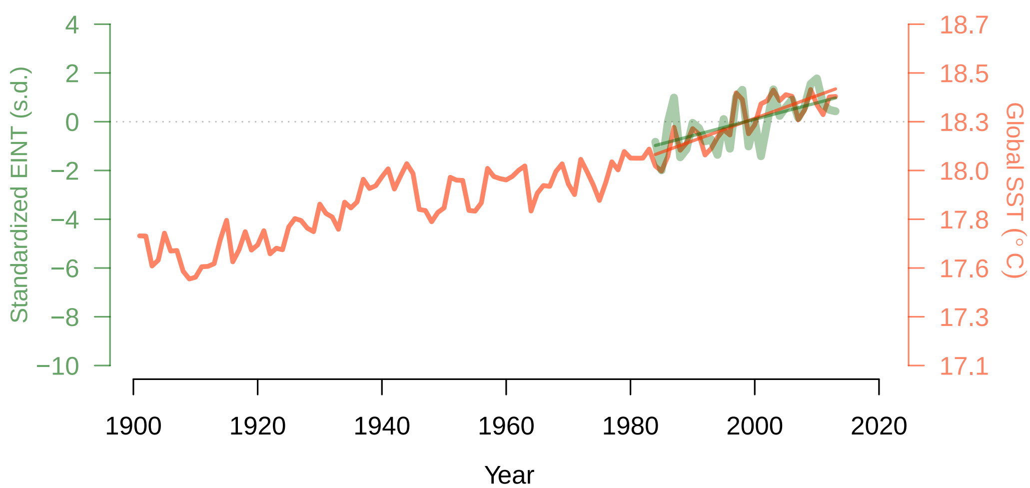

FIG. 6. Time series of global ocean warmth (red line) and EINT (green line) in the western North Pacific. Global mean SST is used to indicate global ocean warmth. Values are standardized to the 30-year period (1984–2013) and the scale for the SST values are presented on the right axis.

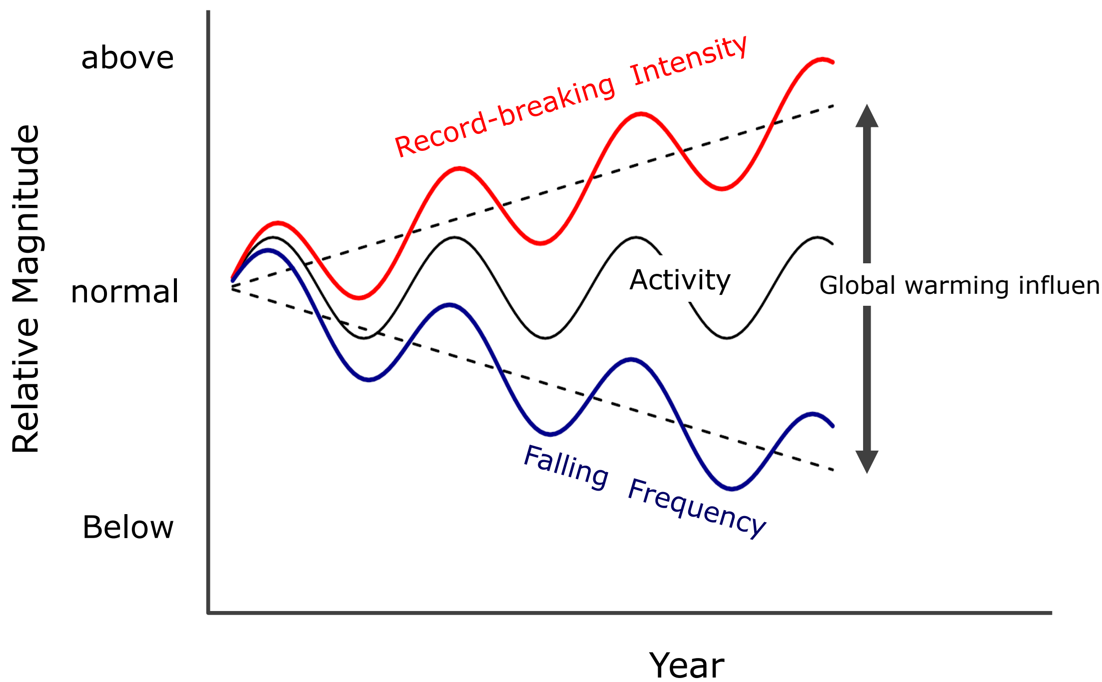

342 FIG. 7. Schematic of global warming's influence on TC climate in the western North Pacific. Intensity variation is the linear combination of activity and efficiency of intensity, while frequency variation is the linear combination of activity and negative efficiency of intensity. Global warming influences the efficiency of intensity rather than activity. From a linear perspective this climate change results in record-breaking intensities with fewer tropical cyclones.

View publication stats